JMEPEG (2017) 26:5571–5576
DOI: 10.1007/s11665-017-2985-z

1059-9495/$19.00

Microstructure and Interfacial Shear Strength in W/$(Zr_{55}Cu_{30}Al_{10}Ni_5)_{100-x}Nb_x$ Composites

M. Mahmoodan, R. Gholamipour, Sh. Mirdamadi, and S. Nategh

(Submitted May 26, 2016; in revised form May 1, 2017; published online October 16, 2017)

In the present study, $(Zr_{55}Cu_{30}Al_{10}Ni_5)_{100-x}Nb_{(x=0,1,2,3)}$ bulk metallic glass matrix/tungsten wire composites were fabricated by a gas pressure infiltration process at temperature 950 °C for 5 min. Microstructural studies and mechanical behaviors of the materials have been investigated by scanning electron microscopy, transmission electron microscopy and pullout tests. The mechanical results showed that the interface shear strength in the composite sample with $X = 2$ increased more than twice compared to the composite sample with $X = 0$. Based on the microstructural results, the addition of two atomic percent Nb in the matrix composite causes an increase in the diffusion band thickness during the melt infiltration and change in the interface fracture mode as a result of pullout test.

Keywords composite, diffusion band, interface shear strength, Nb

1. Introduction

Monolithic bulk metallic glasses (BMGs) generally fail in a catastrophic manner during deformation at room temperature due to the formation of highly localized shear bands (Ref 1-5). In order to achieve an extended ductility, some fabrication methods of BMG composites have been practiced (Ref 6-10). Zr-based BMG matrix composites with various reinforcements were developed to prevent localizing shear strain which caused propagation of multiple shear bands resulting in some ductility improvements (Ref 9-15).

During a melt infiltration process, in Zr-based BMG matrix reinforcement by tungsten wire composites, tungsten diffuses into the matrix and zirconium diffuses into the tungsten fiber leading to formation of diffusion band in the interface of the composite. When a liquid alloy spreads on a tungsten fiber, further interdiffusion may cause higher dissolution of the tungsten fiber resulting in the formation of some crystalline phases present as a layer (known as reaction layer) or particles (called as convection of particles) in the microstructure of the matrix (Ref 2, 13, 16-19).

Generally, the interface properties have a significant effect on the overall structural integrity of the composite. The previous studies showed that the ductility enhancement mechanism in W/BMG matrix composite produced by melt infiltration is different from the other brittle matrix composites. In brittle matrix composites [specifically, in ceramic matrix composites (CMCs)], the increase in ductility in a weak interface can be explained by energy absorption mechanisms where fiber matrix debonding, crack deflection, fiber bridging and fiber pullout are the common mechanisms for preventing the catastrophic failure.

A number of researchers emphasized the shear bands role on the W/BMG composites fracture failure and showed that a weak junction cannot branch the shear bands properly and also the crystalline phases formation during the infiltration process (forming near the interface) acts as the stress concentration sites leading to the rapid conversion of shear bands to cracks as well as the composite fracture. They also indicated that the control of reaction and atomic diffusion at the liquid/solid interface are also necessary for realizing reasonable interfacial bonding strength and preventing the precipitation of brittle intermetallic crystalline phases at the interface (Ref 15, 20-24).

But in the previous studies, the effect of stability or instability of diffusion band and its thickness changes during the infiltration process and also the interface fracture mode during the fiber pullout from the matrix on the W/BMG matrix composites interface shear strength has not been investigated. It seems that some refractory elements such as Nb and Ta can reduce the interface interaction of W/Zr-based BMG matrix composite (Ref 20-22). In this work, the effect of Nb content in BMGs on interface mechanical behavior and microstructural properties of W/BMG interface has systematically been investigated.

2. Experimental

Ingots of $(Zr_{55}Cu_{30}Al_{10}Ni_5)_{100-x}Nb_{(x=0,1,2,3)}$ (at.%) were prepared by arc melting high-purity elements in Ti-gettered and Ar atmosphere on a water-cooled copper crucible. Zr and Nb elements were first melted together, and then other elements were added to the Nb-Zr ingot and remelted several times for homogenizing the alloy. At the last step of remelting, the prepared molten alloy was cast into a water-cooled copper mold (i.e., using suction casting method) to make BMG rods with 4 mm diameters. Schematic infiltration setup during melting process is shown in (Fig. 1). A tungsten wire of 1 mm diameter was straightened and cut into 50 mm length and cleaned in an ultrasonic bath of acetone and ethanol. The tungsten wires were

M. Mahmoodan, **Sh. Mirdamadi**, and **S. Nategh**, Department of Materials Engineering, Science and Research Branch, Islamic Azad University, Tehran, Iran; and **R. Gholamipour**, Department of Advanced Materials and Renewable Energy, Iranian Research Organization for Science and Technology (IROST), P.O. Box 33535111, Tehran, Iran. Contact e-mail: rgholamipour@gmail.com.

placed in parallel at the bottom of sealed 4-mm ID stainless steel tubes (304) (Fig. 2). The tubes were washed by repeated evacuation (up to 10^{-9} MPa) and by purging high-purity Ar gas several times followed by heating at temperature of 950 °C in an electrical furnace and holding for 15 min under a 0.35 MPa Ar pressure. In this condition, molten ingot was infiltrated to the wires and finally they were quenched in water. The volume fraction of W wires was 70%, which was calculated by dividing the wires volume (equal to weight by density of wires) to the mold cavity volume. The pullout tests were performed on tungsten fiber-reinforced $(Zr_{55}Cu_{30}Al_{10}Ni_5)_{100-x}Nb_{(x=0,1,2,3)}$ bulk metallic glass matrix composites. The tensile specimens were cut by a low-speed saw for preparing pullout test samples. Mechanical properties were measured with a SANTAM (STM250) testing machine under (ASTM D-638) standard and speed of 0.048 mm/min. The microstructural observations were carried out by scanning electron microscopy (SEM) and transmission electron microscopy (TEM at 200 kV).

3. Results and Discussion

The TEM micrographs from the matrix and fiber of W/$(Zr_{55}Cu_{30}Al_{10}Ni_5)_{100-x}Nb_{x=2}$ composite sample infiltrated at 950 °C for 15 min are shown in Fig. 3. As can be seen, the selected area diffraction pattern (SADP) image from the matrix confirms that it still remains amorphous after infiltration process.

The backscattered SEM micrographs of the composite samples around the interface are shown in Fig. 4. In Nb-free composites, a diffusion band may be formed at the beginning of the infiltration process, then with the increase in the infiltration time a reaction layer is formed from the diffusion band, after which some particles separate from the reaction layer by convection and disperse in the matrix (see Fig. 4a). In fact, all three mechanisms, i.e., diffusion band, reaction layer and convection of particles, balance each other (Ref 17-19, 22, 25). Table 1 shows the energy-dispersive spectroscopy (EDS) from the convectional particles in Fig. 4(a). Based on the EDS results, the main crystalline phase formed in the composite interface in Fig. 4(a) is W_2Zr. The formation of this crystalline phase has been confirmed by XRD results reported in a previous study (Ref 24).

Figure 4(b) and (c) shows that the diffusion band (D.B) is stable in the composite samples with $X = 1$ and $X = 2$ with thickness of about 4 and 12 micrometers, respectively. However, in the composite sample with $X = 3$ the diffusion band is not stable and converts to the reaction layer, as shown in Fig. 4(d). Formation of the crystalline phase (Al_3Nb) in the matrix and interface of the composite sample with $X = 3$ during the infiltration process probably are the main reason for the instability of diffusion band (Ref 24). The Nb addition (up to 2 at.%) prevents the formation of crystalline phases in the interface of the composite and hinders the interaction between W and Zr because of the strong affinity between W and Nb (mixing = −34 kJ/mol) (Ref 26). The addition of Nb to the matrix decreases the diffusion coefficient of Zr in the matrix during infiltration (Ref 20). Thus, both thermodynamic and kinetic phenomena are the reasons that the interface reaction is restrained (Ref 17, 20, 22).

According to our previous study, the line scanning of an EDS across the matrix to fiber for the composite sample with $X = 2$ (Fig. 6 in Ref 24 showed that in the diffusion band (DB) there is a gradual change in concentration from 100 to zero at.% of tungsten. This means that this kind of D.B acts as a functionally graded layer. The formation of FGM layer in composite interface can improve its mechanical properties significantly (Ref 27). A number of researchers reported that the most important characteristic of functionally graded materials is the ability to inhibit crack propagation because of the lack of stress concentration in functionally graded layer resulted from the continuous microstructure change in this layer compared with a sharp layer (Ref 27-29).

Figure 5 shows the force–distance curves resulted from the pullout test for the composite samples. The value of interface shear strength (τ_d) is given by the equation as (Ref 22):

$$\tau_d = \frac{P_{max}}{2\pi l r_f}$$

where P_{max} is the maximum load (debonding point), r_f is the radius of the fiber, and l is the length of the interaction zone.

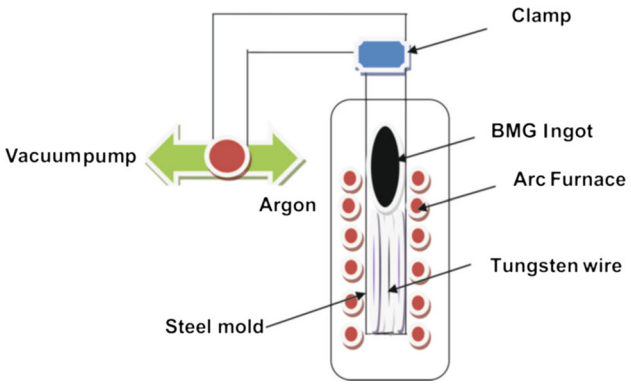

Fig. 1 Schematic infiltration setup during melting process

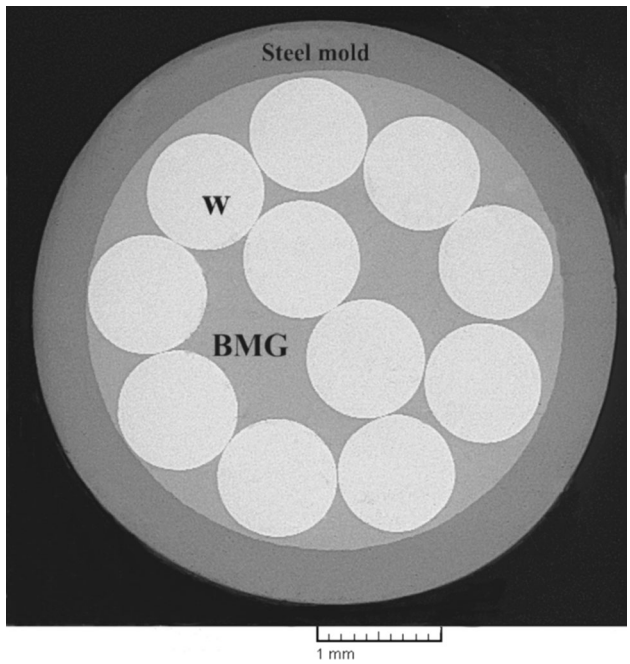

Fig. 2 The cross section of the as-produced composite

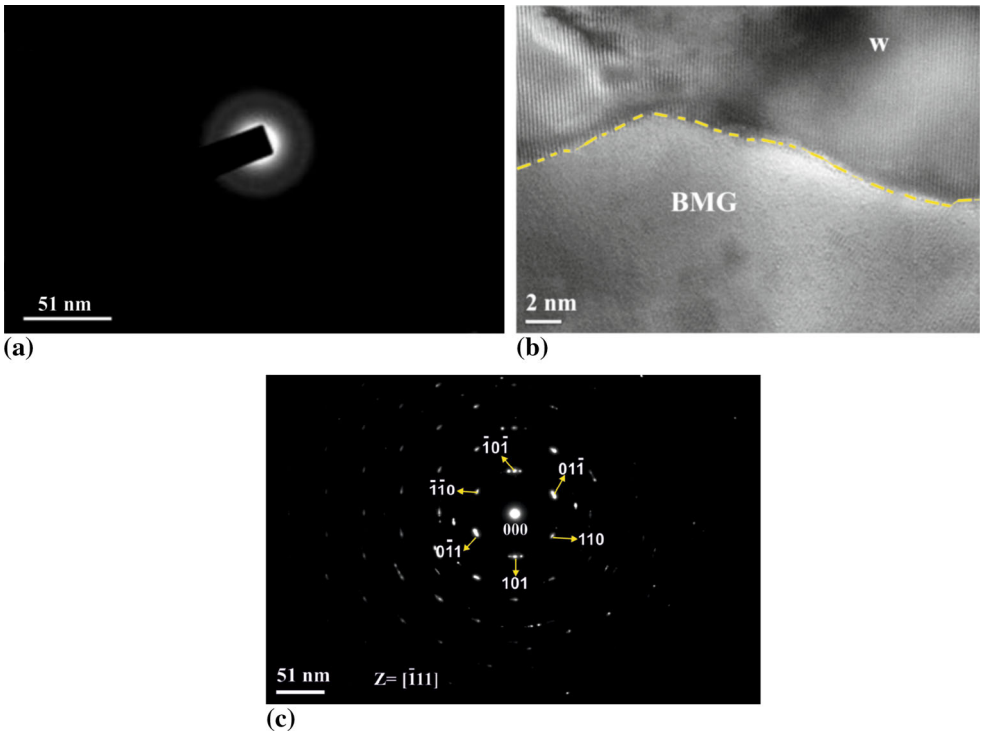

Fig. 3 TEM micrographs from matrix and fiber of W/$(Zr_{55}Cu_{30}Al_{10}Ni_5)_{100-x}Nb_{x=2}$ composite that infiltrated at 950 °C for 15 min, (a) the SADP images of BMG matrix, (b) the bright field image of composite structure and (c) the SADP images of tungsten wire

As shown in Fig. 5, point (a) is known as the debonding point where the load reaches a minimum value required for the debonding of the tungsten wire from the BMG matrix. With an increase in the tensile load, the tungsten wire restarts to come out from the matrix and post-debonding happens at point (b) where due to the friction force between tungsten and BMG matrix the slope of the force–distance curve increases from point (b) to (c). Finally, with the expansion of cracks in the interface and due to the further tungsten wire debonding from the matrix, the composite samples are failed at point (c) and the entire length of the W fiber gets debonded and pulled out of the matrix. The quantitative results extracted from the load–distance curves (Fig. 5) are summarized in Table 2.

As shown in Table 2, the interface shear strength in the composite samples with Nb is higher than the Nb-free composite sample. The best interface shear strength belongs to the composite sample with $X = 2$, and the composite sample with $X = 0$ has the lowest interface shear strength among the composite samples.

The SEM fractography of BMG matrix in point (c) of Fig. 5 is shown in Fig. 6. As can be recognized, there are two regions; the first region is a vein-like pattern, being typical fracture feature for metallic glass. This vein-like pattern often extends along uniform direction which was explained by the local melting within the primary shear band induced by the high elastic energy in the instantaneous fracture. The second region is the smooth pattern where this type of fracture represents the brittle fracture (Ref 17). As shown in Fig. 6, the highest veins density belongs to the composite sample with $X = 2$ (with the best interface shear strength, see Table 1) and the vein-like pattern fracture mode is not seen in the composite sample with $X = 0$ (with the lowest interface shear strength, see Table 1). Some researchers reported that the ductility of BMG matrix composite with the high vein density is more than the composites with low vein density (Ref 17, 21).

As indicated in Fig. 4 and 6, in the composite sample with $X = 2$, with the increase in the diffusion band thickness the veins density has increased compared with the composite sample with $X = 1$. In fact, the higher diffusion band thickness (as a functionally graded layer), the higher crack initiation and propagation restriction. Therefore, more plastic deformation is predicted in the sample with $x = 2$. This higher plastic deformation is due to the higher density of shear bands in microstructure of the metallic glasses. Higher shear bands density causes an increase in the local melting points in fracture surface leading to an increase in the veins density (see Fig. 6c).

As shown in Table 2 and Fig. 4, the formation of reaction layer and convectional particles in composites interface [or instability of diffusion band (D.B)] can play an important role in the degradation of interface shear strength. In the composite samples with $X = 3$ and $X = 0$ due to the reaction layer and convection particles formation and instability of diffusion band, the interface shear strength has been reduced, because of the absence of a mature interface microstructure.

Ma et al. (Ref 22) in their study on tungsten fiber-reinforced $Zr_{41.25}Ti_{13.75}Cu_{12.5}Ni_{10}Be_{22.5}$ metallic glass matrix composites fabricated by means of melt infiltration casting showed that the weak interface between W fibers and matrix cannot transfer load effectively. A number of researchers also have reported that the excessive interface reaction reduced the mechanical properties of the interface. These studies also indicated that high interface strength is needed for the transverse strength of the composite. However, the optimum interface would lead to the improvement of the fiber-reinforced composites' mechanical properties (Ref 9, 15, 20-23, 25). We showed that the composite sample with $X = 2$ has the best mechanical proper-

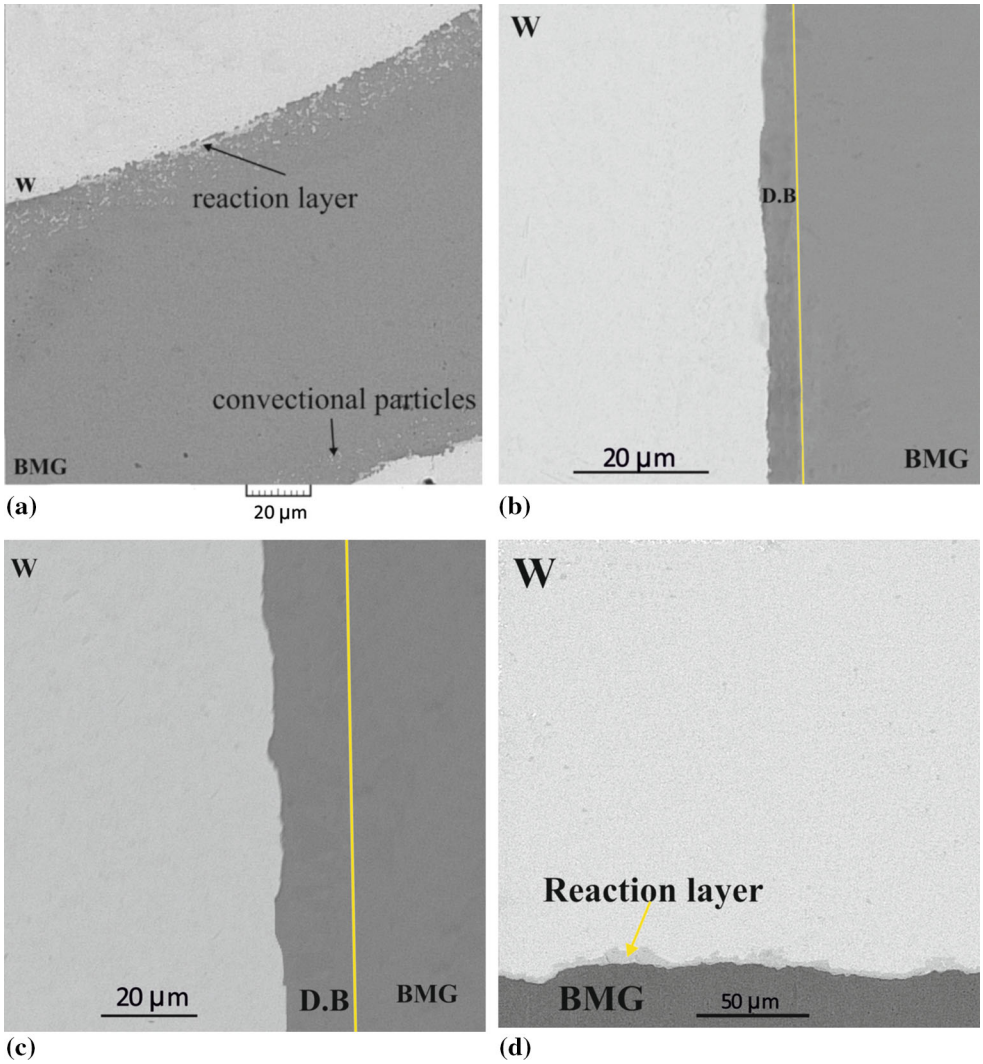

Fig. 4 The SEM backscattered micrographs of W/$(Zr_{55}Cu_{30}Al_{10}Ni_5)_{100-x}Nb_{(x=0,\ 1,\ 2,\ 3)}$ composites that infiltrated at 950 °C for 15 min. (a) $X = 0$, (b) $X = 1$, (c) $X = 2$ and (d) $X = 3$

Table 1 The energy-dispersive spectroscopy (EDS) from the convectional particles in Fig. 4(a)

Element	Norm. C, wt.%	Atom. C, at.%
Aluminum	4.89	16.41
Nickel	2.06	3.17
Copper	10.93	15.57
Tungsten	48.85	48.47
Zirconium	33.27	16.38

ties of 2105 MPa compressive ultimate strength and 28% plastic strain before failure.

The chemical and mechanical bonding formation during infiltration and quenching processes is the source of strengthening of the composites. Chemical bonding is an atomic transport, by diffusion processes, and the compound formation may occur at the interface, resulting in a reinforcement/matrix interfacial zone with a certain thickness. The fiber-reinforced composites with high diffusion band thickness had a strong chemical bonding at the interface (Ref 23). Therefore, the strongest chemical bonding belongs to the composite sample with $X = 2$, while the composite sample with $X = 0$ had the lowest one.

Mechanical bonding is created when the matrix radially shrinks more than the fiber on cooling from high temperature (Ref 23). This would lead to radial gripping stress (σ_r) that is related to the interfacial shear strength (τ_d) by the equation as (Ref 16):

$$\tau_d = \mu\sigma_r$$

where μ is the coefficient of friction, generally between 0.1 and 0.6.

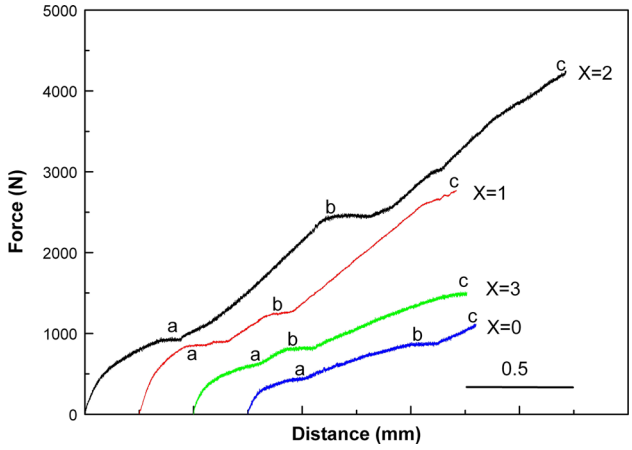

Fig. 5 The line scanning from an energy-dispersive spectroscopy (EDS) across matrix to fiber of $W/(Zr_{55}Cu_{30}Al_{10}Ni_5)_{100-x}Nb_{(x=2)}$ composite

According to the two above-mentioned equations with the assumption of equal friction coefficient in all samples, it can be written as:

Table 2 The pullout test results from $W/(Zr_{55}Cu_{30}Al_{10}Ni_5)_{100-x}Nb_{(x=0,\ 1,\ 2,\ 3)}$ composite samples that infiltrated at 950 °C for 15 min

Composite sample	Interface area, mm^2	Maximum load, Mpa [at point (a) in Fig. 4]	τ_d, Mpa
$X = 0$	6	445	8.85
$X = 1$	5	846	16.83
$X = 2$	5	910	18.10
$X = 3$	5	786	13.03

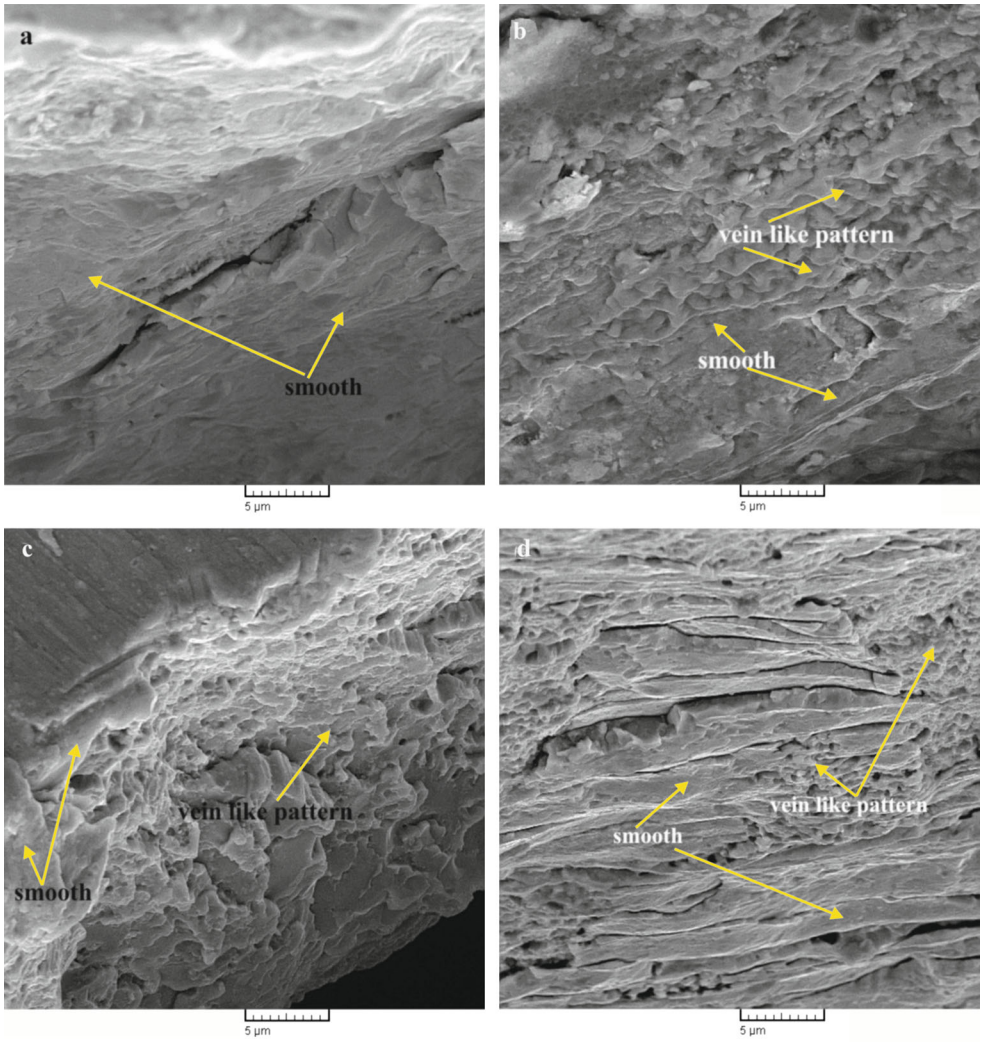

Fig. 6 The force–distance curves resulted from pullout test for $W/(Zr_{55}Cu_{30}Al_{10}Ni_5)_{100-x}Nb_{(x=0,\ 1,\ 2,\ 3)}$ composites that infiltrated at 950 °C for 15 min (a) $X = 0$, (b) $X = 1$, (c) $X = 2$ and (d) $X = 3$. The SEM fractography of BMG matrix in point of pulling the tungsten fiber from the matrix of $W/(Zr_{55}Cu_{30}Al_{10}Ni_5)_{100-x}Nb_{(x=0,\ 1,\ 2,\ 3)}$ composites that in (a) $X = 0$, (b) $X = 1$, (c) $X = 2$ and (d) $X = 3$

$$\sigma_r = \frac{P_{max}}{2\pi\mu l r_f}$$

According to the relationship between the radial gripping stress and the maximum load, it can be concluded that with an increase in the radial gripping stress (σ_r), the load required for the debonding of the tungsten wire from the BMG matrix has increased. The highest P_{max} of the sample with $X = 2$ (see Fig. 5) shows that the mechanical bonding in the interface of the sample is also higher than that of the others.

4. Conclusions

1. The selected area diffraction patterns images (SADP) obtained from TEM showed that the matrix of the composite sample with $X = 2$ was fully amorphous after infiltration process at 950 °C for 15 min.
2. The diffusion band in the composite sample with $X = 1$ and $X = 2$ was stable, but in the composite samples with $X = 3$ and $X = 0$ it was not stable and converts to reaction layer and convectional particles, respectively.
3. The composite samples interface shear strength was strongly related to the interface chemical bonding. So that the composite sample with $X = 2$ and with the highest diffusion band thickness had the highest interface shear strength.

References

1. S.T. Deng and H. Diao, Metallic Glass Fiber Reinforced Zr Based Bulk Metallic Glass, *Scr. Mater.*, 2011, **64**, p 85–88
2. J.W. Qiao, Y. Zhang, P.K. Liaw, and G.L. Chen, Micromechanisms of Plastic Deformation of a Dendrite/Zr-Based Bulk Metallic Composite, *Scr. Mater.*, 2009, **61**, p 1087–1090
3. D. Dargoi, E. Ustundag, B. Clausen, and M.A. Bourke, Investigation of Thermal Residual Stress in Tungsten-Fiber/Bulk Metallic Glass Matrix Composite, *Scr. Mater.*, 2001, **45**, p 245–252
4. F. Abdeljawad, M. Fontus, and M. Haataja, Ductility of Bulk Metallic Glass Composites: Microstructural Effects, *J. Appl. Phys.*, 2011, **98**, p 031909–031909-3
5. R.D. Conner, R.B. Dandliker, V. Scruggs, and W.L. Johnson, Dynamic Deformation Behavior of Tungsten Fiber/Metallic-Glass Matrix Composites, *Int. J. Impact Eng.*, 2000, **24**, p 435–444
6. H. Li and K. Li, Micromechanical Modeling of Tungsten-Based Bulk Metallic Glass Matrix Composites, *Mater. Sci. Eng. A*, 2006, **429**, p 115–123
7. J. Qiao and Y. Zhang, Effect of Nb Content on the Microstructures and Mechanical Properties of Zr-Ti-Cu-Be-Nb Glass-Forming Alloys, *Intermetallics*, 2011, **19**, p 149–153
8. B.Y. Zhang, X. Chen, and S. Wang, High Strength Tungsten Wire Reinforced Zr-Based Bulk Metallic Matrix Composites Prepared by Continuous Infiltration Process, *Mater. Lett.*, 2013, **93**, p 210–214
9. H. Choi, S.Y. Lee, and R.D. Conner, Mechanical Behavior of Mo and Ta Wire Reinforced Bulk Metallic Glass Composites, *Scr. Mater.*, 2008, **58**, p 763–766
10. G.Y. Sun and G. Chen, Comparison of Microstructures and Properties of Zr-Based Bulk Metallic Glass Composites With Dendritic and Spherical bcc Phase Precipitates, *Intermetallics*, 2007, **15**, p 632–634
11. G. Wang, D.M. Chen, J. Shen, Z.H. Stachurski, Q.H. Quin, J.F. Sun, and B.D. Zhou, Deformation Behavior of a Tungsten-Wire, Bulk Metallic Glass Matrix Composite in a Wide Strain Rate Range, *J. Non Cryst. Solids*, 2006, **352**, p 3872–3878
12. D. Singh and R.K. Mandal, Nanoindentation Characteristics of $Zr_{69.5}Al_{7.5-x}Ga_xCu_{12}Ni_{11}$ Glass and their Nanocomposites, *J. Alloys Compd.*, 2011, **509**, p 8657–8663
13. N. Khademian and R. Gholamipour, Fabrication and Mechanical Properties of a Tungsten Wire Reinforced Cu-Zr-Al Bulk Metallic Glass Composite, *Mater. Sci. Eng. A*, 2010, **527**, p 3079–3084
14. K.Q. Qiu, A.M. Wang, H.F. Zhang, B.Z. Ding, and Z.Q. Hu, Mechanical Properties of Tungsten Fiber Reinforced ZrAlNiCuSi Metallic Glass Matrix Composite, *Intermetallics*, 2002, **10**, p 1283–1288
15. Q.S. Zhang, H.F. Zhang, B.Z. Ding, and Z.Q. Hu, Compressive Fracture of $Zr_{55}Cu_{30}Al_{10}Ni_5$ Bulk Amorphous Alloy at High Temperatures, *Mater. Sci. Eng. A*, 2003, **360**, p 280–284
16. X.M. Chun, K.Y. Jia, X. Chen, and Q.Z. Zhi, Interfacial reaction and Bending Strength of SiC/A356/FeNi50 Composite Fabricated by Gas Pressure Infiltration, *Trans. Nonferrous Met. Soc. China*, 2013, **23**, p 2229–2235
17. N. Khademian and R. Gholamipour, Study on Microstructure and Fracture Behavior of Tungsten Wire Reinforced Cu-Based and Zr-Based Bulk Metallic Glass Matrix Composites, *J. Non Cryst. Solids*, 2013, **365**, p 75–84
18. R.D. Conner, H. Choi, and W.L. Johnson, Mechanical Properties of $Zr_{57}Nb_5Al_{10}Cu_{15.4}Ni_{12.6}$ Metallic Glass Matrix Particulate Composites, *J. Mater. Res.*, 1999, **14**, p 3292–3297
19. X. Hui, J. Yu, M. Wang, W. Dong, and G. Chen, Wetting Angle and Infiltration Velocity of Zr Based Bulk Metallic Glass Composite, *Intermetallics*, 2006, **14**, p 931–935
20. M.L. Wang, G.L. Chen, X. Hui, Y. Zhang, and Z.Y. Bai, Optimized Interface and Mechanical Properties of W Fiber/Zr-Based Bulk Metallic Glass Composites by Minor Nb Addition, *Intermetallics*, 2007, **15**, p 1309–1315
21. H. Zhang, H. Li, and A.M. Wang, Synthesis and Characteristics of 80 vol.% Tungsten (W) Fiber/Zr Based Metallic Glass Composite, *Intermetallics*, 2009, **17**, p 1070–1077
22. W.F. Ma, H.C. Kou, C.C. Chen, J.S. Li, R. Hu, L.Q. Xing, L. Zhou, and H.Z. Fu, Interfacial Characteristics and Dynamic Mechanical Properties of W_f/Zr-Based Metallic Glass Matrix Composites, *Trans. Nonferrous Met. Soc. China*, 2013, **18**, p 77–81
23. N. Chawla and K.K. Chawla, *Metal Matrix Composites*, 3rd ed., Springer Press, Berlin, 2006
24. M. Mahmoodan, R. Gholamipour, S. Mirdamadi, and S. Nategh, Effect of Nb Content on Mechanical Behavior and Structural Properties of W/$(Zr_{55}Cu_{30}Al_{10}Ni_5)_{100-x}Nb_x$ Composite, *Metall. Mater. Trans. A*, 2017, **48**, p 2496–2503
25. E. Karimi, R. Gholamipour, and B. Ghasemi, Effect of Melt Infiltration Parameters on Microstructure and Mechanical Properties of Tungsten Wire Reinforced $(Cu50Zr43Al7)_{99.5}Si_{0.5}$ Metallic Glass Matrix Composite, *Trans. Nonferrous Met. Soc. China*, 2015, **25**, p 2624–2629
26. A.R. Miedemax, F.R. Boerxx, and R. Boom, Model Predictions for the Enthalpy of Formation of Transition Metal Alloys, *Calphad*, 1977, **1**, p 341–359
27. S. Suresh and A. Mortensen, Functionally Graded Metals and Metal-Ceramic Composite, *Int. Mater. Rev.*, 1997, **42**, p 85–116
28. C.S. Huang, O.G. Mcgee, and M.J. Chang, Vibrations of Cracked Rectangular FGM Thick Plates, *Compos. Struct.*, 2011, **93**, p 1747–1765
29. L. Lu, M. Chekroun, O. Abraham, V. Maupin, and G. Villain, Mechanical Properties Estimation of Functionally Graded Materials Using Surface Waves Recorded With a Laser Interferometer, *NDT E Int.*, 2011, **44**, p 169–177